crystals

MDPI

Review

Magnetic Force Microscopy of Multiferroic Bulk Ceramic Oxides

Hana Uršič [1,2,*], Matej Šadl [1], Uroš Prah [1,3] and Val Fišinger [1]

[1] Electronic Ceramics Department, Jožef Stefan Institute, Jamova cesta 39, 1000 Ljubljana, Slovenia
[2] Jožef Stefan International Postgraduate School, Jamova cesta 39, 1000 Ljubljana, Slovenia
[3] Materials Research and Technology Department, Luxembourg Institute of Science and Technology, Rue du Brill 41, 4422 Belvaux, Luxembourg
* Correspondence: hana.ursic@ijs.si

Abstract: Bulk multiferroic ceramics have been extensively studied due to their great potential for magneto-electric coupling applications such as low-power and multifunctional nano-electronic devices. In most of these studies the macroscopic magnetic performance was investigated, while the magnetic response on the micro- and nano-scale was not examined in detail. Local magnetic phenomena can be studied using magnetic force microscopy (MFM), a technique derived from atomic force microscopy. MFM measures the magnetic force between the magnetised tip and the magnetic sample. It is one of the most used methods to characterise the structure of ferromagnetic domains, because the sample preparation is simple, non-destructive and provides a relatively high-resolution image. In this review paper we focus on the MFM analyses of bulk multiferroic ceramics. The core of the article is divided into four sections: the introduction, the preparation of samples prior to MFM examination, the reviews of MFM analyses performed on bulk multiferroic ceramics with and without external magnetic fields, and finally the conclusions and an outlook for the future.

Keywords: magnetic force microscopy; multiferroics; bulk ceramic oxides; applied external magnetic field

Citation: Uršič, H.; Šadl, M.; Prah, U.; Fišinger, V. Magnetic Force Microscopy of Multiferroic Bulk Ceramic Oxides. *Crystals* **2023**, *13*, 838. https://doi.org/10.3390/cryst13050838

Academic Editor: Haibo Zhang

Received: 17 April 2023
Revised: 10 May 2023
Accepted: 16 May 2023
Published: 19 May 2023

1. Introduction

Multiferroics are materials where ferroelectric and ferromagnetic, ferrimagnetic or antiferromagnetic ordering can coexist. Multiferroics in bulk ceramic form have a potential in multicaloric applications, which require large quantity of active materials, for example in future caloric cooling applications. Multicaloric effect could represent efficient solid state cooling by magnetic and electric fields in the future [1]. Readers seeking more information about multiferroics should refer to [2–8]. In this review, we focus on the magnetic domain structure of multiferroic oxide bulk ceramics studied by magnetic force microscopy (MFM). The question arises why there are not many MFM studies on multiferroic bulk ceramic materials. The answer lies in three reasons: (1) MFM is still not a widely spread characterization tool, (2) there are only a few multiferroics that exhibit multiferroic properties at room temperature [2,4] and (3) there are far less atomic force microscope (AFM) instruments that allow MFM analysis at cryogenic temperatures [9].

The MFM belongs to the group of scanning-probe microscopies, and dates back to the invention of the scanning-tunnelling microscope by Binnig and Rohrer in 1981. This won them the Nobel Prize in Physics, and was one of the triggers for the era of nanoscience. Five years later, Binnig, Quate and Gerber developed the AFM. From then on, various modes were developed and added to the AFM, e.g., magnetic force microscopy, piezo-response force microscopy, conductive AFM, and electrostatic force microscopy. The MFM was developed in 1987 [10,11].

The AFM consists of the AFM tip on a cantilever, a piezoelectric scanner, a photodiode, a data-acquisition unit and a controller (Figure 1a). The AFM tip, sometimes called the AFM probe, is a sensor that detects the interaction force, i.e., the van der Waals forces, between the tip and the surface of the sample being studied [12]. We can scan the surface

in three different modes: contact mode, tapping mode and non-contact mode. In the first case the AFM tip is in hard contact with the surface. The surface topography is detected by the deflection of the cantilever from its original position, which is monitored by the reflection of a laser from the photodiode. When scanning in tapping mode, the AFM tip is periodically in contact or not with the surface of the sample. In non-contact mode, the tip has no contact with the surface at all and the surface is detected only by the long-range interaction forces between the tip and the sample [13].

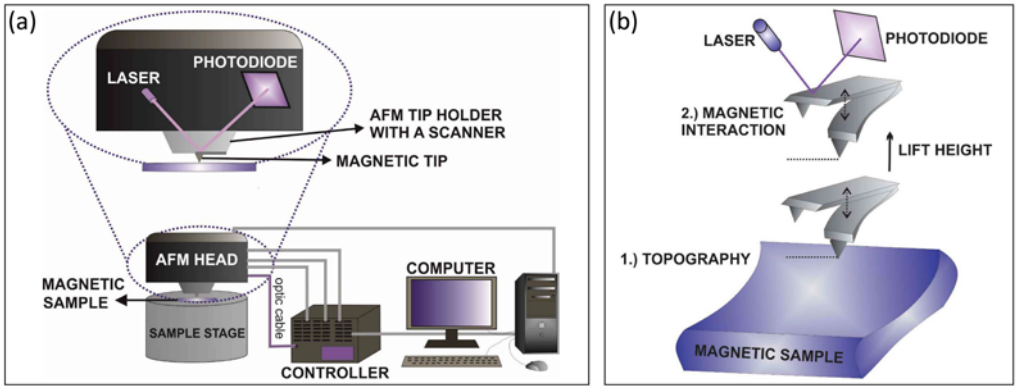

Figure 1. (**a**) Example of AFM system adapted for MFM measurements. (**b**) Schematic of the MFM measurement principle.

In MFM, the interaction force is the magnetic force between the magnetised tip and the magnetic sample. In addition to magnetic interactions, van der Waals interaction forces are also present. These are responsible for the topography signal in the tapping and non-contact modes. The signal contains both magnetic and topographic information. To separate these two signals, the two-pass technique is normally applied. The dominant force depends on the distance of the tip from the sample. The van der Waals forces are short-range forces, while the magnetic forces act over longer distances between the tip and the surface (i.e., tens of nanometres). Therefore, by scanning images at different heights we can separate the magnetic and topographic signals. In the two-pass technique, the sample is scanned twice. In the first pass, the topography (i.e., a height profile) is determined, usually by tapping-mode scanning. In the second scan, the distance between the tip and the sample is increased, while the tip maintains the same height profile as in the first scan. In this way the distance and van der Waals interactions between the cantilever and the sample surface remain constant. In this case the tip is subject only to changes in the magnetic interactions, resulting in an MFM image. The principle of the two-pass MFM technique is shown in Figure 1b.

In the second scan when there are no magnetic interactions between the sample and the tip the cantilever oscillates with frequency v_1, amplitude a_1, and phase ϕ_1. However, when a magnetic interaction occurs between the magnetic sample and the MFM tip, the cantilever starts to oscillate with frequency v_2, amplitude a_2, and phase ϕ_2. Therefore, the change in the magnetic interaction is monitored by shifts in the frequency ($\Delta v = v_1 - v_2$), amplitude ($\Delta a = a_1 - a_2$), and phase ($\Delta\phi = \phi_1 - \phi_2$). Usually, an MFM image is presented as Δv or $\Delta\phi$ scans. The changes in frequency and phase are related to the magnetic interactions between the tip and the sample (F) according to the following equations [9]:

$$\Delta v \approx -\frac{v_1}{2k}\frac{dF}{dz} \quad (1)$$

$$\Delta\phi \approx \frac{Q}{k}\frac{dF}{dz} \quad (2)$$

where z is the cantilever displacement and Q and k are the quality factor and the spring constant of the cantilever, respectively. An overview of the different approaches to quantify MFM signals can be found here [9].

Figure 2 shows some examples of MFM frequency, amplitude and phase-signal images of a glass slide, a computer hard disk and a videotape. The glass is a non-magnetic material that serves as a reference material. As expected, only noise is observed in the MFM signals of the glass slide (Figure 2c–e). The MFM frequency, amplitude and phase images of the hard disk (Figure 2h–j) and videotape (Figure 2m–o) show magnetic features that are not related to the topographic height or any deflection of the sample surfaces (Figure 2f,g,k,l). The MFM scans of the hard disk and videotape show periodic magnetic domains, which is consistent with the literature [14,15]. The most sensitive rendition of the magnetic domain structure is achieved in MFM frequency images.

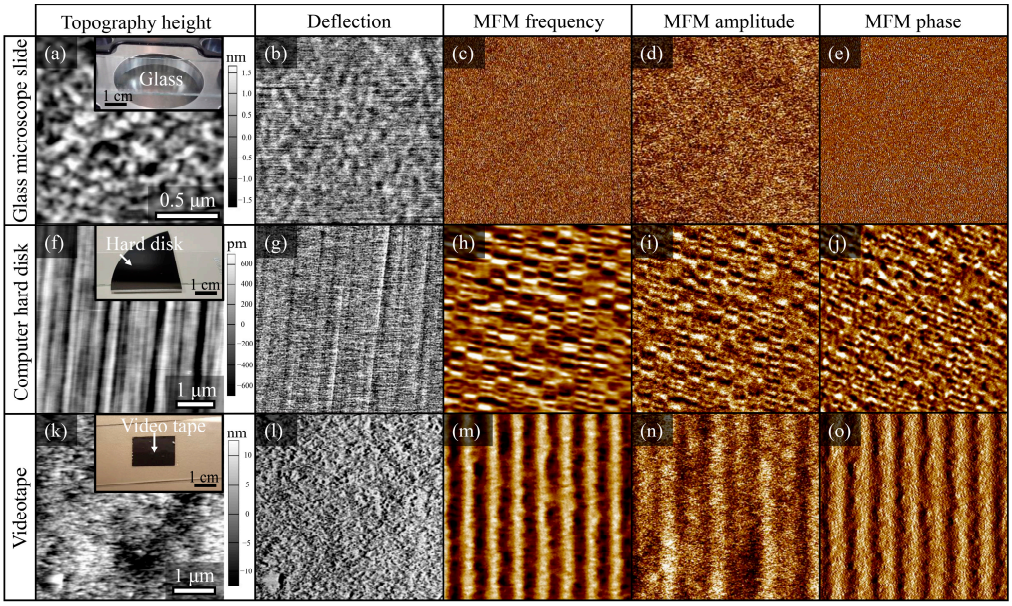

Figure 2. AFM topographic height, deflection and MFM frequency v, amplitude a and phase ϕ signal images of (**a**–**e**) glass slide, (**f**–**j**) computer hard disk (Maxtor D740X-6L 40GB HDD) and (**k**–**o**) videotape.

There are two options for the MFM tips: they can be made entirely of magnetic materials, such as iron, or they can be standard AFM tips that are coated with magnetic materials (e.g., CoCr, CoPt, FePt and NiFe alloys). Prior to the MFM measurements, the MFM tip must be magnetised to detect the magnetic interactions. Magnetisation can be achieved by bringing a permanent magnet close to a pristine MFM tip. To further confirm that the detected signal does indeed correlate with the magnetic properties of the material under investigation, an experiment can be performed with the opposite polarity of the tip (Figure 3a). Two scans of the same area can be performed. Before the first scan, the MFM tip is magnetised using a specific pole of the external magnet, while before the second scan, the MFM tip is magnetised with the opposite pole of the magnet. If the comparison of the two scans shows an inverted MFM signal, this is confirmation that the MFM signal results from the magnetic properties of the sample and is not due to crosstalk with the topography, an electrostatic contribution, or other experimental errors (Figure 3b). The removal of electrostatic artifacts by controlled magnetisation of the MFM tip is studied in more detail in [16].

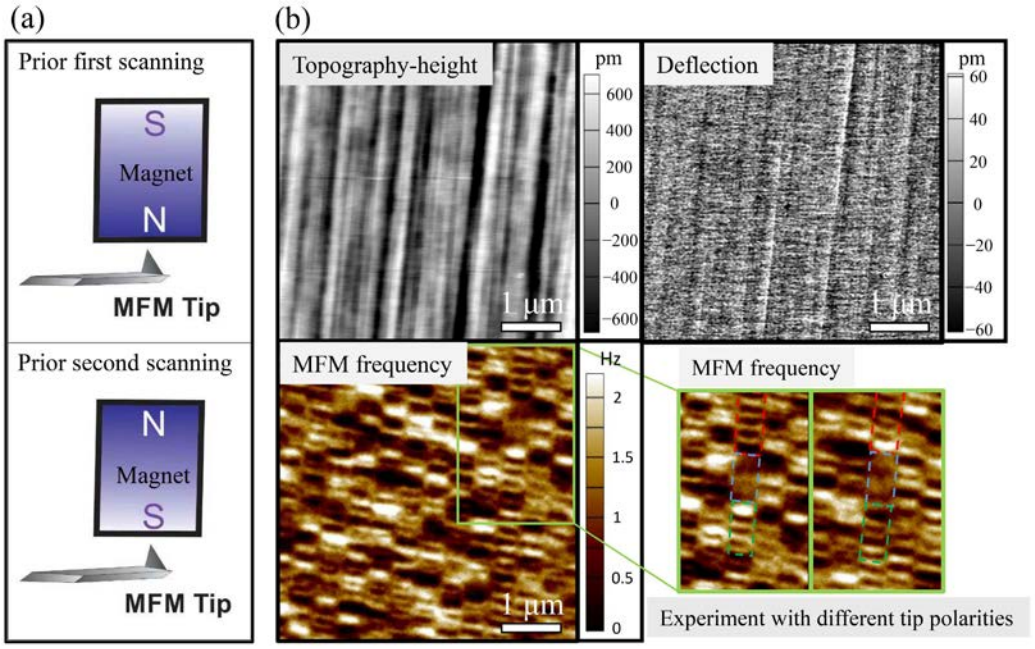

Figure 3. (**a**) Schematic of the experiment with different tip polarities. (**b**) AFM topographic height and deflection images and MFM frequency images of a computer hard disk. The green rectangle highlights a region where an experiment with opposite magnetic tip polarities was performed. The pairs of coloured dashed brackets represent the same region with an inverted MFM signal.

2. Polishing and Cleaning of Multiferroic Ceramic Specimens Prior to MFM Analysis

The MFM analysis of multiferroic thin films can be performed without pre-treatment [17–21], because the thin films are flat with the roughness below or in nanometre range. On the other hand, single crystals or bulk ceramics must be cut and polished [22–25]. Proper polishing and cleaning of crystal or ceramic samples are necessary to obtain the roughness of the samples below micrometre range and therefore to minimize the cross-talk of the MFM signal with the topography, leading to high-quality MFM images. A similar polishing-and-cleaning procedure for the bulk samples is also required for high-quality piezo-response force microscopy (PFM) images, as explained in [13].

The ceramics are usually cut to the correct dimensions and polished to obtain a flat surface for the MFM examination. The procedure requires several steps. The first is embedding the ceramic sample in polymer resin, for example in epoxy resin (Figure 4a), and grinding with silicon-carbide abrasive papers (5–20 μm SiC particles). The second step is polishing the sample on a cloth with a polishing paste, gradually reducing the size of the diamond abrasive to 0.25 μm. The third step is fine polishing with a colloidal SiO_2 suspension containing particles down to tens of nanometres (Figure 4b) [22]. The bulk sample is then removed from the epoxy resin by heating so that the epoxy resin softens and the sample can be removed (Figure 4c,d). The sample is then prepared for MFM measurements (Figure 4e). One option is also to coat the surface of the multiferroic sample with a gold layer a few tens of nanometres thick to eliminate the electrostatic interactions between the ferroelectric domains and the MFM tip [26].

Surface contamination between the MFM tip and the multiferroic sample can interfere with the magnetic signal, as shown in Figure 5. The sample can be cleaned with an ultrasonic cleaner, UV ozone cleaner, lens-cleaning cloth or acetone, depending on the type of sample and the surface contaminants. Note, however, that acetone can leave stains on the surface of the sample. Removing contaminants is not always easy, so it is advantageous to work in a dust-free area such as a clean room.

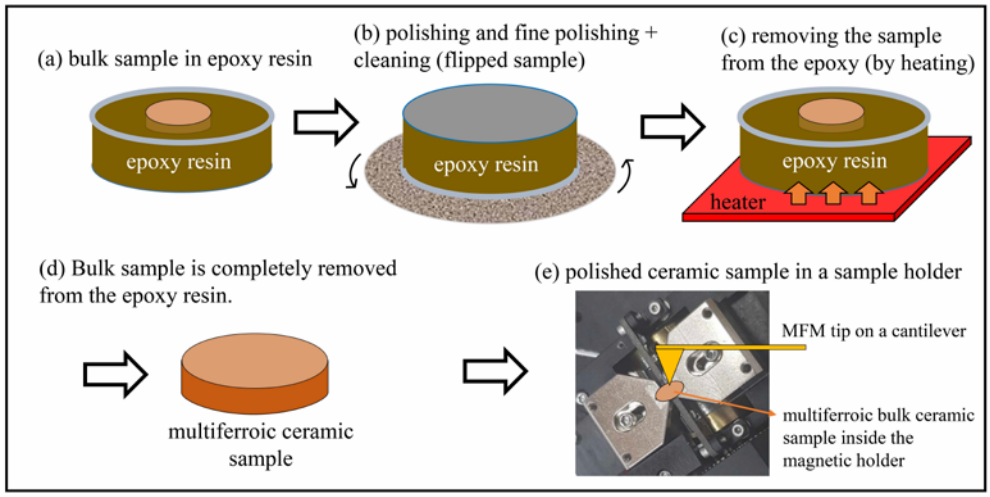

Figure 4. Schematic of a multiferroic bulk ceramic sample's preparation prior to MFM investigation.

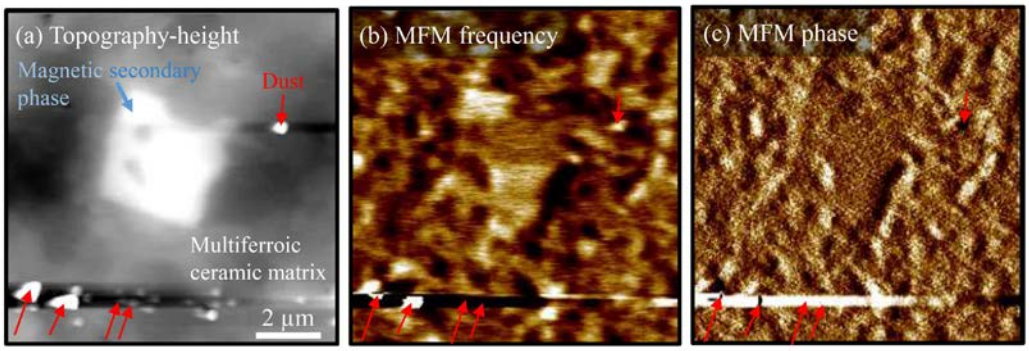

Figure 5. (**a**) AFM topography height and MFM (**b**) frequency and (**c**) phase images of a $Bi_{0.88}Gd_{0.12}FeO_3$ multiferroic ceramic containing an Fe-rich secondary phase after polishing with a paste on a cloth and fine polishing with a colloidal SiO_2 suspension. Some examples of dust particles on the sample surface are marked with red arrows.

3. MFM Studies of Magnetic Domains in Multiferroic Bulk-Ceramic Samples

We focus here on the MFM of ceramic samples of multiferroic oxide. There are only a few studies on this topic [22,27–30], as discussed in more detail below. Other investigations deal with the MFM of multiferroic thin films [17–21,31–33], single crystals [25,26,34,35], nanowires [36,37], composites and heterostructures [23,24,27,38,39], all of which are beyond the scope of this review.

A large group of single-phase multiferroic materials is based on the bismuth ferrite $BiFeO_3$ (BFO), which exhibits antiferromagnetic ordering with a Néel temperature of ~380 °C and ferroelectric behaviour with a ferroelectric Curie temperature of ~825 °C [40]. Rare-earth-element-modified BFOs are interesting because they can exhibit an enhanced ferromagnetic response compared to the parent BFO [22]. Their multiferroic domain structure, i.e., ferroelectric and magnetic domains, can be observed by PFM and MFM, as shown in Figure 6f–k for $Bi_{0.88}Gd_{0.12}FeO_3$ ceramics. The PFM out-of-plane amplitude and phase images (Figure 6f,g) show the ferroelectric domain structure of the BFO matrix and the non-piezoelectric Fe-rich secondary phase. On the other hand, the MFM frequency and phase images show that both the BFO matrix and the Fe-rich secondary phase are magnetic (Figure 6h,i). As is shown here, microstructural analysis using MFM plays a crucial role in the characterization and interpretation of macroscopic magnetic measurements. The MFM experiment with opposite tip polarities (Figure 6j,k) shows an inverted MFM frequency signal (highlighted by the arrows) of the BFO matrix and the Fe-rich secondary phase, proving that the sample–tip interaction is indeed magnetic and not the result of topography or other non-magnetic phenomena.

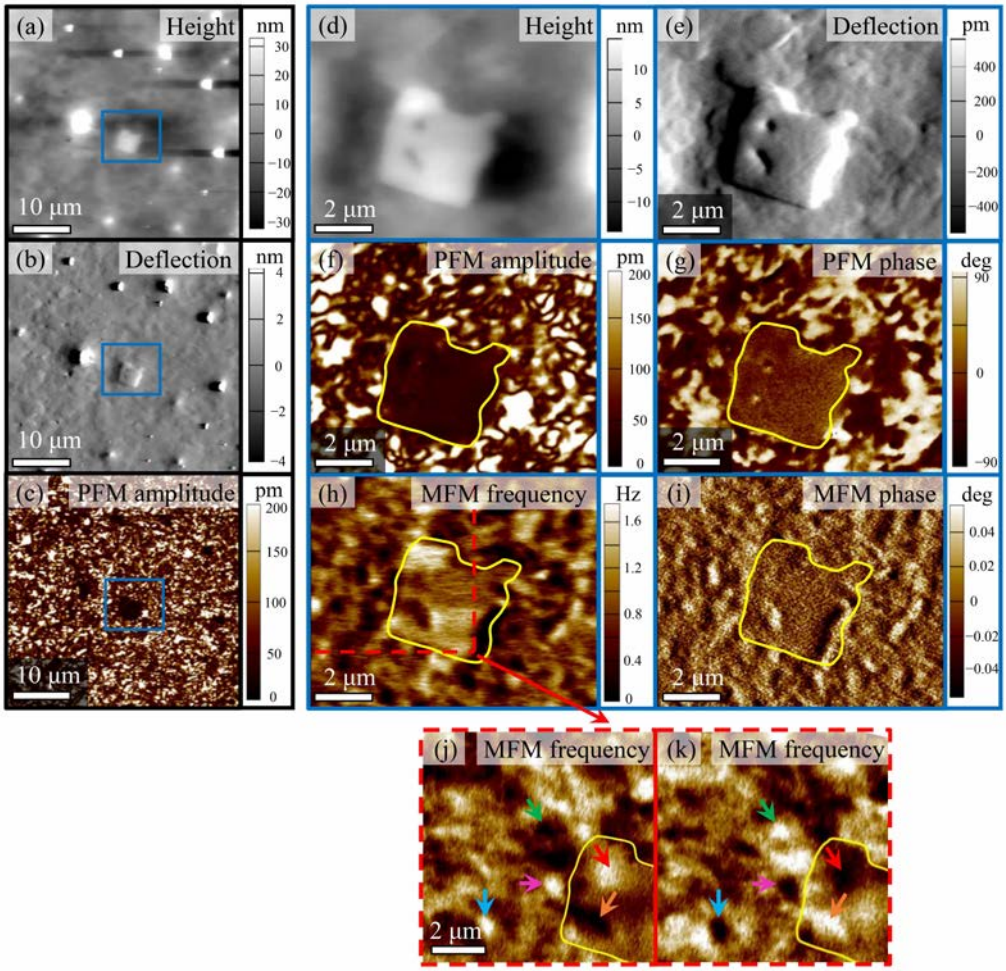

Figure 6. (**a**,**b**) AFM topography height and deflection and (**c**) PFM amplitude images of $Bi_{0.88}Gd_{0.12}FeO_3$ bulk ceramics. The blue square marks a region of Fe-rich secondary phase, magnified in panels (**d**–**i**) and indicated by a yellow line. Panels (**f**,**g**) show PFM amplitude and phase images, and (**h**,**i**) show MFM frequency and phase images of this region. Panels (**j**,**k**) show MFM frequency of a region where an experiment with opposite magnetic tip polarities was performed [22]. Copyright 2020 Elsevier (Creative Commons CC-BY license).

A MFM analysis of the Li-modified BFO ceramic $Li_xBi_{1-x}FeO_3$ with x = 0.03 and x = 0.09 is also reported in the literature [27]. An X-ray diffraction analysis revealed that the $Li_{0.09}Bi_{0.91}FeO_3$ ceramic prepared by convectional solid-state synthesis contains two secondary phases, namely $LiFe_5O_8$ (15 vol%) and $Bi_{12.5}Fe_{0.5}O_{20}$ (6.2 vol%). MFM experiments on this sample revealed magnetic domains from nanometre to micrometre size. The density of the magnetic domains decreased with decreasing Li concentration from x = 0.09 to 0.03 [27]. In addition, a MFM analysis was performed on $Bi_{0.85}Sm_{0.15}Fe_{0.97}Sc_{0.03}O_3$ ceramics prepared by hot pressing [28]. Long-range magnetic ordering was observed in these samples at room temperature (Figure 7). In a similar way, the long-range magnetic ordering was observed in Nd-modified BFO ceramics ($Bi_{1-x}Nd_xFeO_3$) with high Nd concentrations (x > 0.14) [29].

The microstructural investigation of bulk ceramics by MFM is very important to distinguish different phenomena between the matrix and the inclusions. A very interesting features in relaxor ferroelectrics are polar nanoregions that have the ability to form ferroelectric and magnetic regions, also known as multiferroic clusters (MFC) [30]. In relaxor ferroelectric single-phase $(BiFe_{0.9}Co_{0.1}O_3)_{0.4}$–$(Bi_{1/2}K_{1/2}TiO_3)_{0.6}$ ceramics, the MFC originate from magnetically strong Bi(Fe,Co)O_3-rich regions with sizes in the range of 0.5–1.5 µm (Figure 8). Using the MFM technique a magnetic dipolar response of the

MFC was confirmed by the switching an external (out-of-plane) magnetic field (±0.48 T) (Figure 8c–e). In addition, the MFM signal was altered by an in situ DC electric field (20 V) poling (Figure 8e,f, converse magnetoelectric effect). The direct magnetoelectric effect was also confirmed and even quantified for the MFC by using PFM and a variable external magnetic field [30].

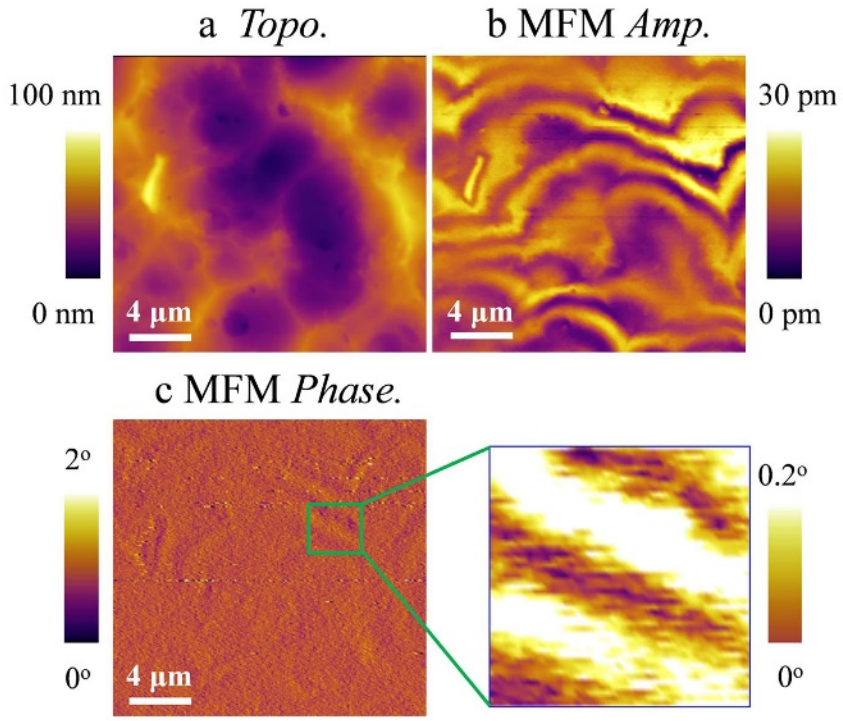

Figure 7. MFM analysis of $Bi_{0.85}Sm_{0.15}Fe_{0.97}Sc_{0.03}O_3$ ceramics. (**a**) AFM topography, MFM (**b**) amplitude and (**c**) phase images [28]. Copyright 2017 Elsevier.

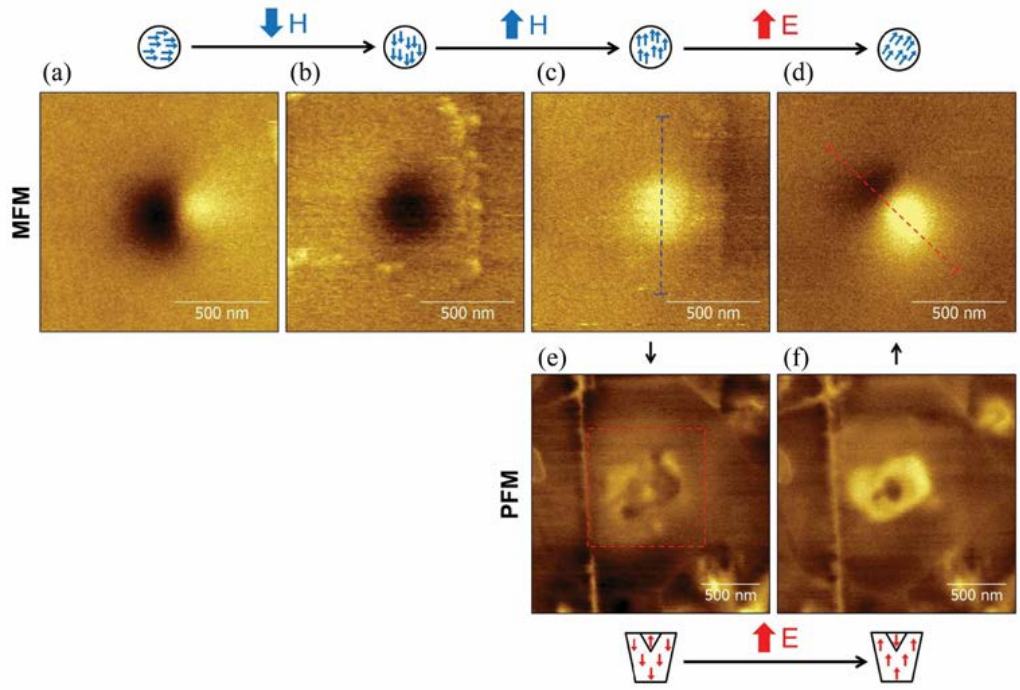

Figure 8. MFM measurements of MFC in relaxor ferroelectric single-phase $(BiFe_{0.9}Co_{0.1}O_3)_{0.4}$–$(Bi_{1/2}K_{1/2}TiO_3)_{0.6}$ ceramics in combination with external magnetic field (*H*) and electric field (*E*) poling.

(**a**–**c**) MFM phase images of the MFC (**a**) before and (**b**,**c**) after ex situ switching with out-of-plane magnetic fields of ±0.48 T as indicated by blue arrows. The symbols above the images represent single magnetic domains according to the dipolar magnetic MFM response. (**e**,**f**) PFM images of MFC recorded after ex situ magnetic switching, (**e**) before and (**f**) after electric field (20 V) poling by scanning a rectangular area as indicated by the red dashed rectangle. Configurations of MFC's polarization are illustrated by symbols below the PFM images. (**d**) MFM phase image after electric field poling, showing magnetoelectric switching [30]. Copyright 2016 Wiley.

One must be very careful when interpreting MFM results, especially when the experiment involves in situ electric field poling. Liu et al. [39] have used in situ electric field poling on thin film $BiFeO_3/La_{0.67}Sr_{0.33}MnO_3$ heterostructures, which resulted not only in a strong contrast of the PFM signal (Figure 9c), but also in a strong contrast of the MFM phase signal (Figure 9d). However, the "magnetic" signal of the MFM phase image does not originate from the electric-field-induced magnetization (converse magnetoelectric coupling), but from electrostatic interactions between the sample surface and the MFM tip, which arise due to the excess surface charges during the poling process. The electrostatic interactions were confirmed by scanning Kelvin probe microscopy (SKPM) in Figure 9e. Moreover, a solution to neutralize the excess surface charges was proposed, namely, scanning the poled region several times with a grounded tip in contact mode [39]. Although this example shows that excess surface charges are introduced into thin films by poling with an electric field, a similar phenomenon can also occur in polished bulk ceramic samples.

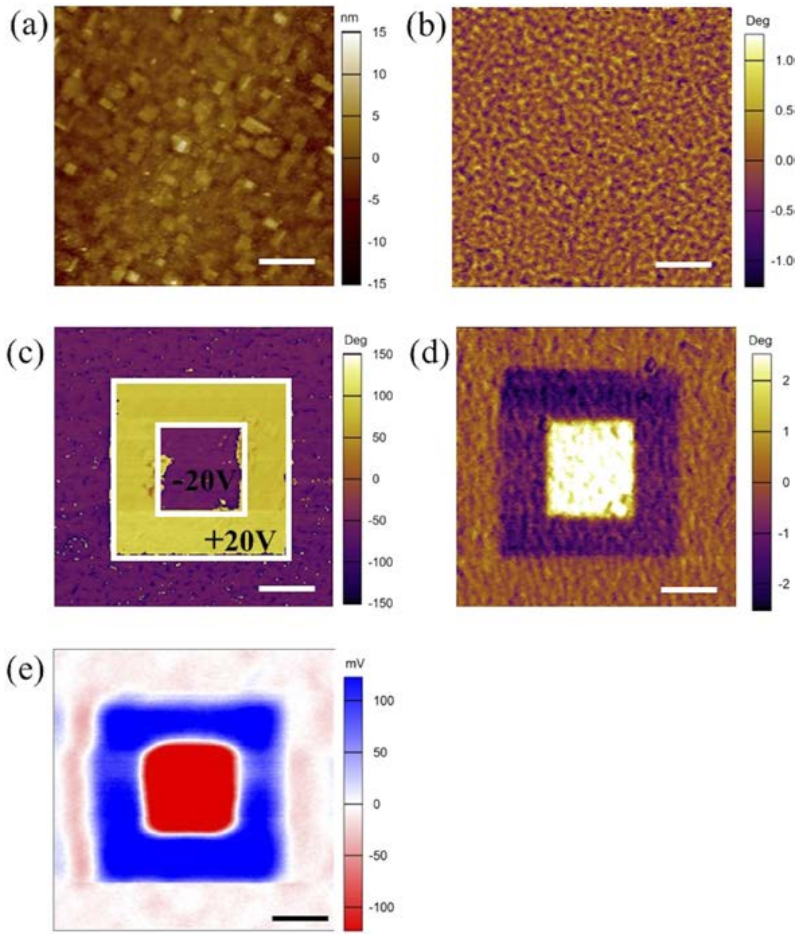

Figure 9. (**a**) AFM topography image and (**b**) MFM phase image of thin film $BiFeO_3/La_{0.67}Sr_{0.33}MnO_3$ heterostructure in the initial state. Figures (**c**–**e**) show (**c**) out-of-plane PFM phase image, (**d**) MFM phase image and (**e**) SKPM potential image, respectively, after double-box polarization. Scale bars represent 1 μm [39]. Copyright 2017 AIP Publishing.

4. Magnetic-Force Microscopy Measurements under an Applied External Magnetic Field

Atomic force microscopes can be equipped with options for applying external magnetic fields to specimens, including out-of-plane and in-plane magnetic fields. With this option, the magnetic domain structure of the materials can be studied inside or outside the external magnetic field. Such a setup is shown schematically in Figure 10, where the magnetic field applied to the sample depends on the rotation angle of the magnet. When the angle of rotation is zero, the magnetic flux is deflected away from the sample. When the magnet is rotated 90°, the magnetic flux is directed through the sample [14,41].

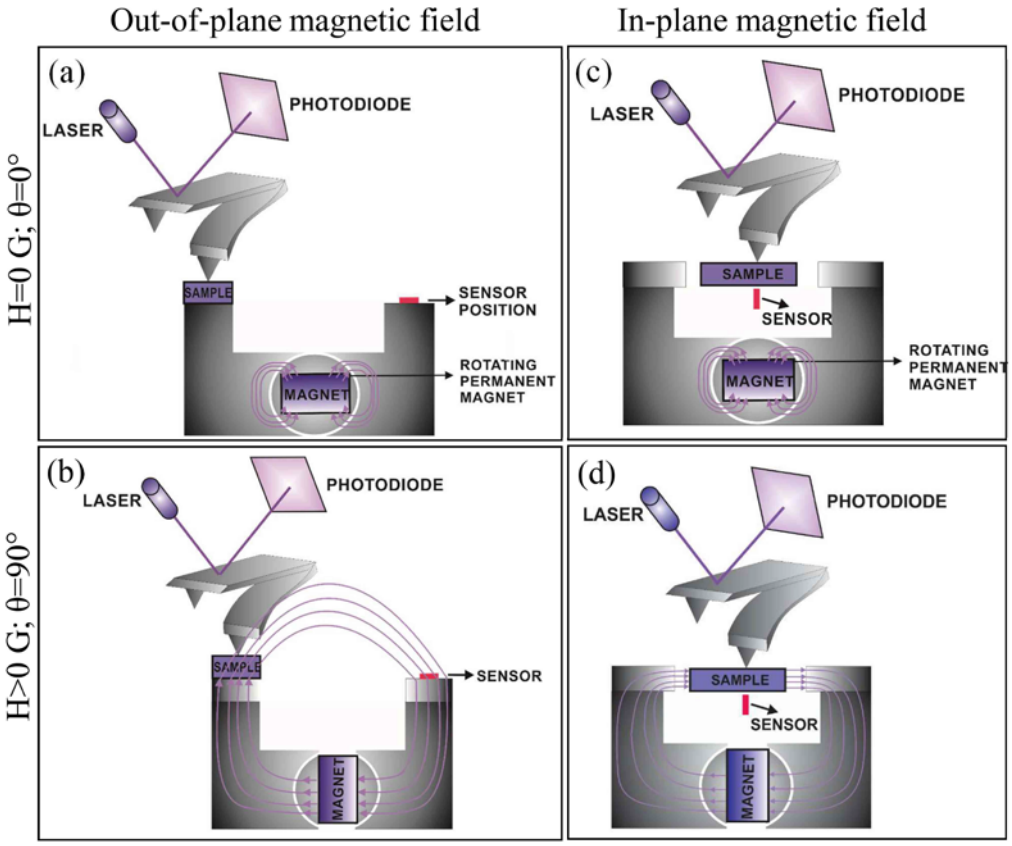

Figure 10. Schematic of the experimental setup for (**a**,**b**) out-of-plane and (**c**,**d**) in-plane magnetic field measurements. When the rotation angle of the magnet is zero, no external magnetic field is applied to the sample, as shown in panels (**a**,**c**). After the magnet is rotated 90°, the sample is brought into the external magnetic field, as shown in panels (**b**,**d**).

Figure 11 shows MFM frequency images of the computer hard disk and the $Bi_{0.88}Gd_{0.12}FeO_3$ bulk ceramic. The images were acquired at in-plane external magnetic fields from 0 G to 7000 G and −7000 G. The ferromagnetic domain structure of the hard disk remains unchanged up to 4300 G, while at a higher external magnetic field of 7000 G, the ferromagnetic domains switch and become more irregularly shaped. In contrast, the magnetic domains of the $Bi_{0.88}Gd_{0.12}FeO_3$ bulk ceramic do not switch, even at the highest magnetic field of 7000 G. When we change the polarity of the external magnetic field (from 7000 G to −7000 G), we can observe an interesting phenomenon. The MFM experiment on the $Bi_{0.88}Gd_{0.12}FeO_3$ bulk ceramic (Figure 11b, compare 7000 G and −7000 G) shows a complete inversion of the MFM frequency signal, while the shape of the magnetic domain structure remains the same. This indicates, first, that the MFM signal is related to the magnetic interaction between the sample and the tip, and not to the topography cross-talk [14], and, second, that switching of the in-plane external magnetic field causes a change in the polarity of the tip rather than the movements of the ferromagnetic domain walls of the

$Bi_{0.88}Gd_{0.12}FeO_3$. The domain structure of $Bi_{0.88}Gd_{0.12}FeO_3$ ceramics is stable due to the high coercive magnetic field of this sample [22].

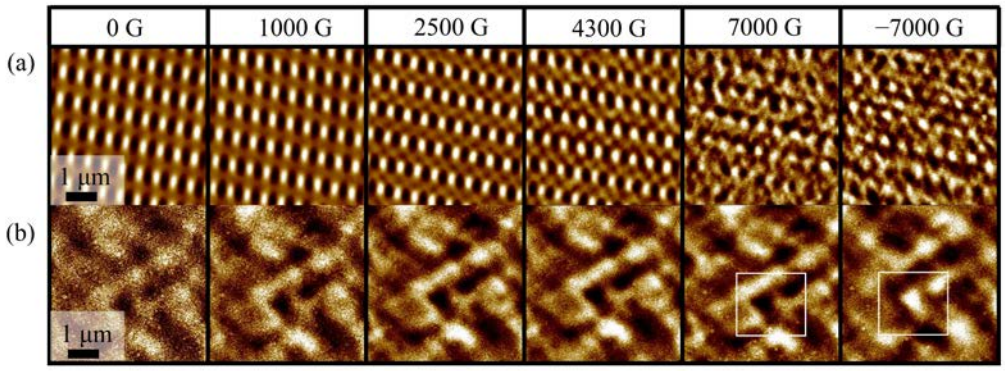

Figure 11. MFM frequency images under external in-plane magnetic fields for (**a**) computer hard disk (Maxtor D740X-6L 40GB HDD) and (**b**) $Bi_{0.88}Gd_{0.12}FeO_3$ bulk ceramics. Measurements were performed using an AFM Jupiter, Asylum Research, Santa Barbara, USA with a MFM tip Asymfmlc-R2. The white square is only a guide for the eyes.

5. Conclusions and Outlook

Our understanding of the multiferroic properties of ceramic materials has improved in recent decades [4–7]. However, there are still many topics that require further research. These include (I) the coupling of the electromechanical and magnetic response in ceramic multiferroics and (II) multiferroic films in cross-section.

The first topic is important because it relates to the coupling of the electromechanical and magnetic responses in ceramic multiferroics at the nanoscale/microscale. An example of such an experiment is shown in Figure 12. The ferroelectric domain structure of the $Bi_{0.88}Gd_{0.12}FeO_3$ bulk ceramic is shown in Figure 12a and is consistent with previous reports [22,42]. The contrasting bright and dark regions in the amplitude images correspond to areas with higher and lower piezoelectric responses. When the sample is subjected to an in-plane external magnetic field, as schematically shown in Figure 12g, the ferroelectric domain structure of the multiferroic $Bi_{0.88}Gd_{0.12}FeO_3$ bulk ceramic does not change, even when the magnetic field is switched to the negative direction. This is related to the low magnetoelectric coefficients at room temperature [43,44] and the high coercive electric field of Gd-modified $BiFeO_3$ ceramics [42].

The second idea for future work in this area is to study multiferroic thick films by MFM in cross-section. The procedure for preparing the thick film specimen prior to MFM examination differs slightly from the procedure for preparing the ceramic specimen shown in Figure 4. Therefore, Figure 13 shows a schematic of this idea. The multiferroic films can be cut in half (Figure 13b,c), embedded in epoxy resin (Figure 13d), and polished in cross-section (Figure 13e). After polishing, the surfaces of the specimens should be cleaned, preferably with distilled water, and dried in air. The specimens are removed from the cast by cutting away the epoxy resin around the films (Figure 13f,g). The specimen is placed in a specimen holder with a polished cross-sectional surface on top (Figure 13h). In the last step, MFM scanning should be performed on the cross-sectional surface. Using a PFM mode, a similar experiment was performed for ferroelectric thick films, where the ferroelectric properties of $0.65Pb(Mg_{1/3}Nb_{2/3})O_3–0.35PbTiO_3$ thick films in cross-section were investigated [45].

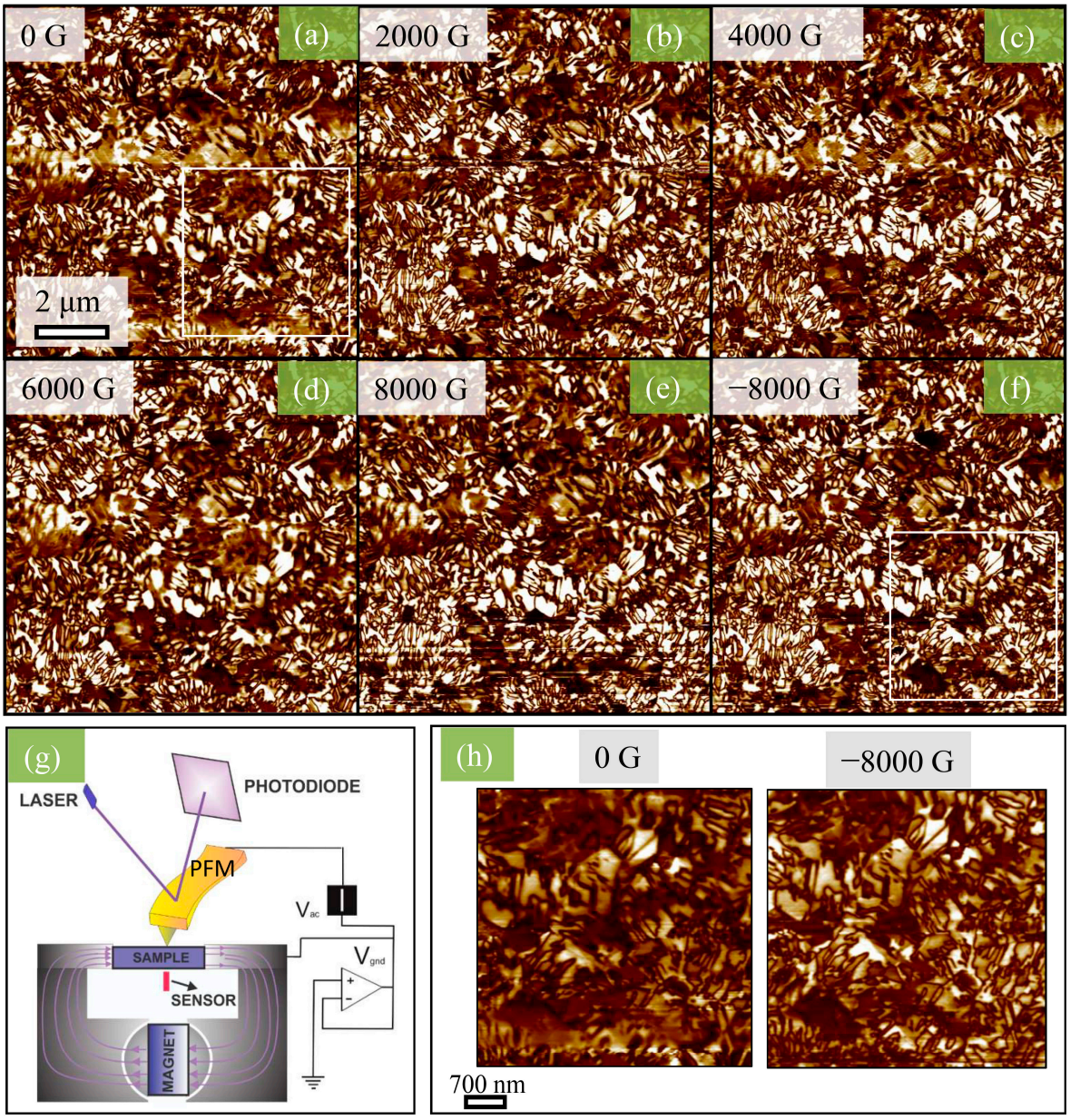

Figure 12. Piezo-response force microscopy of $Bi_{0.88}Gd_{0.12}FeO_3$ bulk ceramics in an external in-plane magnetic field. (**a**–**f**) PFM out-of-plane amplitude image under external in-plane magnetic field from 0 to ±8000 G. (**g**) Schematic representation of the setup for PFM measurements in a magnetic field. (**h**) Enlarged view of the areas marked by the white square in panels (**a**,**f**).

In conclusion, we believe that MFM analyses combined with other techniques such as piezo-response force microscopy, electrostatic force microscopy, conductive atomic force microscopy, thermal scanning microscopy and others, can lead to a deeper understanding and provide a link between the fundamental and functional properties of multiferroic ceramic materials and films at the nanoscale in the future.

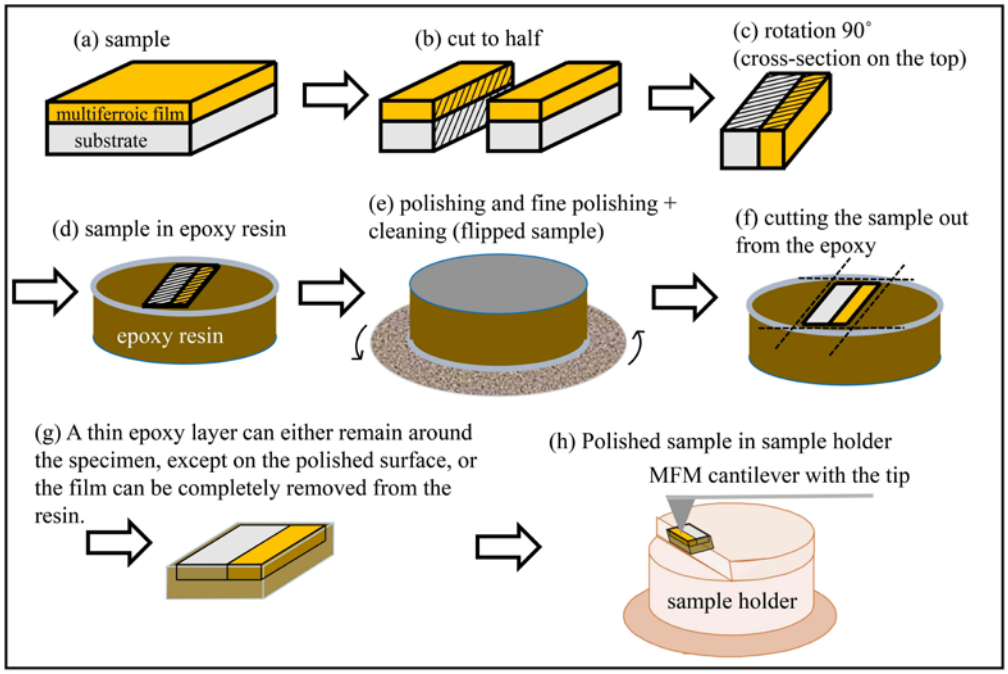

Figure 13. Schematic of a multiferroic thick-film sample's preparation prior to MFM cross-section investigation.

6. Materials and Methods

Figures 2, 3, 5, 11 and 12 were scanned using MFP-3D and Jupiter XR atomic force microscopes, Oxford Instruments, Asylum Research, Santa Barbara, CA, USA. For MFM scanning, the two-pass MFM technique and Si tips coated with CoCr (ASYMFMHM, AtomicForce F&E GmbH, Mannheim, Germany) and Fe (ASYMFMLC, AtomicForce F&E GmbH, Germany) were used. PFM imaging was performed in dual AC resonance tracking mode. A voltage of 5 V and a frequency of ~350 kHz were used. Pt-coated silicon tips with a radius of curvature of ~10 nm (OMCL-AC240TM-R3, Olympus, Tokyo, Japan) were used.

Author Contributions: Conceptualisation, H.U.; methodology, H.U., M.Š., U.P. and V.F.; investigation, H.U., U.P. and V.F.; data curation, H.U., U.P. and V.F.; writing—original draft preparation, H.U.; writing—review and editing, H.U., M.Š., U.P. and V.F.; visualisation, H.U. and V.F.; supervision, H.U. All authors have read and agreed to the published version of the manuscript.

Funding: This work is funded by the Slovenian Research Agency in the frame of project N2-0212 and research core funding P2-0105.

Data Availability Statement: The data presented in this study are available upon request from the corresponding author.

Acknowledgments: The authors would like to thank Jena Cilenšek, Antonio Lisičak, Maria Karypidou for their help with the graphic design and Julian Walker for $Bi_{0.88}Gd_{0.12}FeO_3$ bulk ceramic sample.

Conflicts of Interest: The authors declare no conflict of interest.

References

1. Vopson, M.M. The multicaloric effect in multiferroic materials. *Solid State Commun.* **2012**, *152*, 2067–2070. [CrossRef]
2. Eerenstein, W.; Mathur, N.D.; Scott, J.F. Multiferroic and magnetoelectric materials. *Nature* **2006**, *442*, 759–765. [CrossRef] [PubMed]
3. Fiebig, M.; Lottermoser, T.; Meier, D.; Trassin, M. The evolution of multiferroics. *Nat. Rev. Mater.* **2016**, *1*, 16046. [CrossRef]
4. Spaldin, N.A.; Ramesh, R. Advances in magnetoelectric multiferroics. *Nat. Mater.* **2019**, *18*, 203–212. [CrossRef] [PubMed]
5. Jia, T.; Cheng, Z.; Zhao, H.; Kimura, H. Domain switching in single-phase multiferroics. *Appl. Phys. Rev.* **2018**, *5*, 021102. [CrossRef]
6. Ramesh, R.; Manipatruni, S. Electric field control of magnetism. *Proc. R. Soc. A* **2021**, *477*, 20200942. [CrossRef]
7. Evans, D.M.; Garcia, V.; Meier, D.; Bibes, M. Domains and domain walls in multiferroics. *Phys. Sci. Rev.* **2020**, *5*, 20190067. [CrossRef]

8. Vopson, M.M. Fundamentals of Multiferroic Materials and Their Possible Applications. *Crit. Rev. Solid State Mater. Sci.* **2015**, *40*, 223–250. [CrossRef]
9. Kazakova, O.; Puttock, R.; Barton, C.; Corte-León, H.; Jaafar, M.; Neu, V.; Asenjo, A. Frontiers of magnetic force microscopy. *J. Appl. Phys.* **2019**, *125*, 060901. [CrossRef]
10. Martin, Y.; Wickramasinghe, H.K. Magnetic imaging by "force microscopy" with 1000 Å resolution. *Appl. Phys. Lett.* **1998**, *50*, 1455. [CrossRef]
11. Sáenz, J.J.; García, N.; Grütter, P.; Meyer, E.; Heinzelmann, H.; Wiesendanger, R.; Rosenthaler, L.; Hidber, H.R.; Güntherodt, H.-J. Observation of magnetic forces by the atomic force microscope. *J. Appl. Phys.* **1987**, *62*, 4293–4295. [CrossRef]
12. Sugawara, Y. Atomic Force Microscopy. In *Roadmap of Scanning Probe Microscopy*; Seizo Morita, Ed.; Springer: Berlin/Heidelberg, Germany, 2007; pp. 15–21. ISBN 978-3-540-34315-8.
13. Uršič, H.; Prah, U. Investigations of ferroelectric polycrystalline bulks and thick films using piezoresponse force microscopy. *Proc. R. Soc. A* **2019**, *475*, 20180782. [CrossRef] [PubMed]
14. Passeri, D.; Angeloni, L.; Reggente, M.; Rossi, M. Magnetic Force Microscopy. In *Magnetic Characterization Techniques for Nanomaterials*; Kumar Challa, S.S.R., Ed.; Springer: Berlin/Heidelberg, Germany, 2017; pp. 209–259. ISBN 9783662527801.
15. Scheunert, G.; Cohen, S.R.; Kullock, R.; McCarron, R.; Rechev, K.; Kaplan-Ashiri, I.; Bitton, O.; Dawson, P.; Hecht, B.; Oron, D. Grazing-incidence optical magnetic recording with super-resolution. *Beilstein J. Nanotechnol.* **2017**, *8*, 28–37. [CrossRef]
16. Angeloni, L.; Passeri, D.; Reggente, M.; Mantovani, D.; Rossi, M. Removal of electrostatic artifacts in magnetic force microscopy by controlled magnetization of the tip: Application to superparamagnetic nanoparticles. *Sci. Rep.* **2016**, *6*, 26293. [CrossRef]
17. Gupta, S.; Pal, M.; Tomar, M.; Guo, R.; Bhalla, A.; Gupta, V. Ferroelectric and magnetic domain mapping of magneto-dielectric Ce doped $BiFeO_3$ thin films. *J. Alloys Compd.* **2021**, *882*, 160698. [CrossRef]
18. Jia, T.; Kimura, H.; Cheng, Z.; Zhao, H. Switching of both local ferroelectric and magnetic domains in multiferroic $Bi_{0.9}La_{0.1}FeO_3$ thin film by mechanical force. *Sci. Rep.* **2016**, *6*, 31867. [CrossRef] [PubMed]
19. Shimizu, K.; Kawabe, R.; Hojo, H.; Shimizu, H.; Yamamoto, H.; Katsumata, M.; Shigematsu, K.; Mibu, K.; Kumagai, Y.; Oba, F.; et al. Direct Observation of Magnetization Reversal by Electric Field at Room Temperature in Co-Substituted Bismuth Ferrite Thin Film. *Nano Lett.* **2019**, *19*, 1767–1773. [CrossRef]
20. Gao, M.; Viswan, R.; Tang, X.; Leung, C.M.; Li, J.; Viehland, D. Magnetoelectricity of $CoFe_2O_4$ and tetragonal phase $BiFeO_3$ nanocomposites prepared by pulsed laser deposition. *Sci. Rep.* **2018**, *8*, 323. [CrossRef]
21. You, L.; Wang, B.; Zou, X.; Lim, Z.S.; Zhou, Y.; Ding, H.; Chen, L.; Wang, J. Origin of the uniaxial magnetic anisotropy in $La_{0.7}Sr_{0.3}MnO_3$ on stripe-domain $BiFeO_3$. *Phys. Rev. B* **2013**, *88*, 184426. [CrossRef]
22. Walker, J.; Mirjanic, A.; Prah, U.; Sadl, M.; Condurache, O.A.; Bencan, A.; Rojac, T.; Grigoras, M.; Ursic, H. Magnetic contributions in multiferroic gadolinium modified bismuth ferrite ceramics. *Scr. Mater.* **2020**, *188*, 233–237. [CrossRef]
23. Shvartsman, V.V.; Alawneh, F.; Borisov, P.; Kozodaev, D.; Lupascu, D.C. Converse magnetoelectric effect in $CoFe_2O_4$–$BaTiO_3$ composites with a core–shell structure. *Smart Mater. Struct.* **2011**, *20*, 075006. [CrossRef]
24. Etier, M.; Shvartsman, V.V.; Gao, Y.; Landers, J.; Wende, H.; Lupascu, D.C. Magnetoelectric Effect in (0–3) $CoFe_2O_4$–$BaTiO_3$(20/80) Composite Ceramics Prepared by the Organosol Route. *Ferroelectrics* **2013**, *448*, 77–85. [CrossRef]
25. Jalli, J.; Hong, Y.K.; Abo, G.S.; Bae, S.; Lee, J.J.; Park, J.H.; Choi, B.C.; Kim, S.G. MFM studies of magnetic domain patterns in bulk barium ferrite ($BaFe_{12}O_{19}$) single crystals. *J. Magn. Magn. Mater.* **2011**, *323*, 2627–2631. [CrossRef]
26. Geng, Y.; Lee, N.; Choi, Y.J.; Cheong, S.-W.; Wu, W. Collective Magnetism at Multiferroic Vortex Domain Walls. *Nano Lett.* **2012**, *12*, 6055–6059. [CrossRef]
27. Sharma, Y.; Agarwal, R.; Collins, L.; Zheng, Q.; Ievlev, A.V.; Hermann, R.P.; Cooper, V.R.; KC, S.; Ivanov, I.N.; Katiyar, R.S.; et al. Self-Assembled Room Temperature Multiferroic $BiFeO_3$–$LiFe_5O_8$ Nanocomposites. *Adv. Funct. Mater.* **2020**, *30*, 1906849. [CrossRef]
28. Wang, C.; Yang, L.; Li, Z.; Zeng, M.; Zhang, A.; Qin, M.; Lu, X.; Gao, X.; Gao, J.; Lam, K.H. Giant room temperature multiferroicity and domain structures in hot-press sintered $Bi_{0.85}Sm_{0.15}Fe_{0.97}Sc_{0.03}O_3$ ceramics. *Ceram. Int.* **2017**, *43*, 12764–12769. [CrossRef]
29. Chen, J.; Xu, B.; Liu, X.Q.; Gao, T.T.; Bellaiche, L.; Chen, X.M. Symmetry Modulation and Enhanced Multiferroic Characteristics in $Bi_{1-x}Nd_xFeO_3$ Ceramics. *Adv. Funct. Mater.* **2019**, *29*, 1806399. [CrossRef]
30. Henrichs, L.F.; Cespedes, O.; Bennett, J.; Landers, J.; Salamon, S.; Heuser, C.; Hansen, T.; Helbig, T.; Gutfleisch, O.; Lupascu, D.C.; et al. Multiferroic Clusters: A New Perspective for Relaxor-Type Room-Temperature Multiferroics. *Adv. Funct. Mater.* **2016**, *26*, 2111–2121. [CrossRef]
31. Keeney, L.; Maity, T.; Schmidt, M.; Amann, A.; Deepak, N.; Petkov, N.; Roy, S.; Pemble, M.E.; Whatmore, R.W. Magnetic Field-Induced Ferroelectric Switching in Multiferroic Aurivillius Phase Thin Films at Room Temperature. *J. Am. Ceram. Soc.* **2013**, *96*, 2339–2357. [CrossRef]
32. Faraz, A.; Maity, T.; Schmidt, M.; Deepak, N.; Roy, S.; Pemble, M.E.; Whatmore, R.W.; Keeney, L. Direct visualization of magnetic-field-induced magnetoelectric switching in multiferroic aurivillius phase thin films. *J. Am. Ceram. Soc.* **2017**, *100*, 975–987. [CrossRef]
33. Li, L.; Lu, L.; Zhang, D.; Su, R.; Yang, G.; Zhai, J.; Yang, Y. Direct Observation of Magnetic Field Induced Ferroelectric Domain Evolution in Self-Assembled Quasi (0–3) $BiFeO_3$–$CoFe_2O_4$ Thin Films. *ACS Appl. Mater. Interfaces* **2016**, *8*, 442–448. [CrossRef] [PubMed]

34. Geng, Y.; Wu, W. Magnetoelectric force microscopy based on magnetic force microscopy with modulated electric field. *Rev. Sci. Instrum.* **2014**, *85*, 053901. [CrossRef] [PubMed]
35. Geng, Y.; Das, H.; Wysocki, A.L.; Wang, X.; Cheong, S.-W.; Mostovoy, M.; Fennie, C.J.; Wu, W. Direct visualization of magnetoelectric domains. *Nat. Mater.* **2014**, *13*, 163–167. [CrossRef] [PubMed]
36. Prashanthi, K.; Shaibani, P.M.; Sohrabi, A.; Natarajan, T.S.; Thundat, T. Nanoscale magnetoelectric coupling in multiferroic $BiFeO_3$ nanowires. *Phys. Status Solidi Rapid Res. Lett.* **2012**, *6*, 244–246. [CrossRef]
37. Prashanthi, K.; Thundat, T. In situ study of electric field-induced magnetization in multiferroic $BiFeO_3$ nanowires. *Scanning* **2014**, *36*, 224–230. [CrossRef]
38. Zavaliche, F.; Zheng, H.; Mohaddes-Ardabili, L.; Yang, S.Y.; Zhan, Q.; Shafer, P.; Reilly, E.; Chopdekar, R.; Jia, Y.; Wright, P.; et al. Electric Field-Induced Magnetization Switching in Epitaxial Columnar Nanostructures. *Nano Lett.* **2005**, *5*, 1793–1796. [CrossRef]
39. Liu, C.; Ma, J.; Ma, J.; Zhang, Y.; Chen, J.; Nan, C.-W. Cautions to predicate multiferroic by atomic force microscopy. *AIP Adv.* **2017**, *7*, 055003. [CrossRef]
40. Catalan, G.; Scott, J.F. Physics and Applications of Bismuth Ferrite. *Adv. Mater.* **2009**, *21*, 2463–2485. [CrossRef]
41. Sylum Reasearch, "Variable Magnetic Field Module". 2021. Available online: https://afm.oxinst.com/products/mfp-3d-other-driving-forces-acccessories/variable-magnetic-field-module (accessed on 27 March 2023).
42. Walker, J.; Ursic, H.; Bencan, A.; Malic, B.; Simons, H.; Reaney, I.; Viola, G.; Nagarajan, V.; Rojac, T. Temperature dependent piezoelectric response and strain-electric-field hysteresis of rare-earth modified bismuth ferrite ceramics. *J. Mater. Chem. C* **2016**, *4*, 7859–7868. [CrossRef]
43. Tryhuk, V.V.; Ravinski, A.F.; Makoed, I.I.; Lazenka, V.V.; Januszkiewicz, K.I. Magnetoelectric Coupling and Lattice Dynamics of Gd-Doped $BiFeO_3$ Multiferroics. In Proceedings of the IEEE International Conference on Oxide Materials for Electronic Engineering (OMEE), Lviv, Ukraine, 3–7 September 2012; pp. 253–254.
44. Pattanayak, S.; Choudhary, R.N.P.; Shannigrahi, S.R.; Das, P.R.; Padhee, R. Ferroelectric and ferromagnetic properties of Gd-modified $BiFeO_3$. *J. Magn. Magn. Mater.* **2013**, *341*, 158–164. [CrossRef]
45. Ursic, H.; Sadl, M. Investigation of piezoelectric $0.65Pb(Mg_{1/3}Nb_{2/3})O_3$–$0.35PbTiO_3$ films in cross section using piezo-response force microscopy. *Appl. Phys. Lett.* **2022**, *121*, 192905. [CrossRef]